The architectural relationship of components controlling mast cell endocytosis

Cédric Cleyrat[1,2], Anza Darehshouri[1,2], Karen L. Anderson[3], Christopher Page[3], Diane S. Lidke[1,2], Niels Volkmann[3], Dorit Hanein[3] and Bridget S. Wilson[1,2,*]

[1]Department of Pathology University of New Mexico Health Sciences Center, Albuquerque, NM 87131, USA
[2]Cancer Center, University of New Mexico Health Sciences Center, Albuquerque, NM 87131, USA
[3]Bioinformatics and Systems Biology Program, Sanford-Burnham Medical Research Institute, La Jolla, CA 92037, USA
*Author for correspondence (bwilson@salud.unm.edu)

Accepted 5 August 2013
Journal of Cell Science 126, 4913–4925

doi: 10.1242/jcs.128876

Summary

Eukaryotic cells use multiple routes for receptor internalization. Here, we examine the topographical relationships of clathrin-dependent and clathrin-independent endocytic structures on the plasma membranes of leukemia-derived mast cells. The high affinity IgE receptor (FcεRI) utilizes both pathways, whereas transferrin receptor serves as a marker for the classical clathrin-mediated endocytosis pathway. Both receptors were tracked by live-cell imaging in the presence or absence of inhibitors that established their differential dependence on specific endocytic adaptor proteins. The topology of antigen-bound FcεRI, clathrin, dynamin, Arf6 and Eps15-positive structures were analyzed by 2D and 3D immunoelectron microscopy techniques, revealing their remarkable spatial relationships and unique geometry. We conclude that the mast cell plasma membrane has multiple specialized domains for endocytosis. Their close proximity might reflect shared components, such as lipids and adaptor proteins, that facilitate inward membrane curvature. Intersections between these specialized domains might represent sorting stations that direct cargo to specific endocytic pathways.

Key words: FcεRI, Endocytosis, CME, CIE, Arf6, Eps15, Mast cell

Introduction

The endocytosis field has reached an important and critical stage, as several decades of work have led to new appreciation of the complex network of adaptor proteins involved in classical clathrin-mediated endocytosis (CME) (Traub, 2009), as well as the intimate relationship between receptor internalization and signal transduction (Sorkin and von Zastrow, 2009). In addition, there is now abundant evidence for clathrin-independent (CIE) receptor internalization pathways (Doherty and McMahon, 2009; Kirkham et al., 2005). These alternative pathways mediate the endocytosis of receptors important in immune regulation, such as the IL-2Rα and γc cytokine receptors (Lamaze et al., 2001; Sauvonnet et al., 2005).

The spatial relationships and interconnectivity between the various players in the CME and CIE pathways is of keen interest. Prior evidence suggests that the endocytic efficiency and/or route for specific receptors depends on complex factors such as aggregation state (Andrews et al., 2009; Liu et al., 2010; Mellman and Plutner, 1984) or ligand dose (Sigismund et al., 2005). The best-known example of a receptor that utilizes both CME and CIE pathways is the epidermal growth factor receptor (EGFR) (Sigismund et al., 2005; Sorkin and von Zastrow, 2009). For the CME pathway alone, at least four distinct and interactive mechanisms converge to regulate EGFR uptake, endosomal signaling and degradation (Goh et al., 2010). Another class of receptors that utilize multiple internalization pathways is the immunoreceptor tyrosine-based activation motif (ITAM)-containing superfamily of immunoreceptors, which includes T-cell antigen receptors (TCRs), B-cell antigen receptors (BCRs) and activating Fc receptors (Martínez-Martín et al., 2011). For example, BCRs and high affinity IgE receptors (FcεRI) can take the alternative internalization pathway in cells that are conditionally depleted of clathrin (Fattakhova et al., 2006; Stoddart et al., 2005). The general characteristics of CIE pathways include: (1) sensitivity to cholesterol depletion; (2) dependence on dynamin and actin; (3) association with lipid rafts; and (4) potential involvement of other components, such as Arf6, Eps15 and epsin, RhoA and/or flotillin-1 (Chadda et al., 2007; Glebov et al., 2006; Lamaze et al., 2001; Naslavsky et al., 2004; Radhakrishna and Donaldson, 1997; Sigismund et al., 2005; Stoddart et al., 2005). Clathrin-independent carriers have been described as uncoated tubular or ring-shaped structures (Kirkham et al., 2005).

The ‘rip-flip’ technique (Sanan and Anderson, 1991), which yields well-preserved membrane sheets that can be labeled with immunogold and imaged by transmission electron microscopy (TEM), has not yet been fully exploited for its unique view of the plasma membrane–cytoplasm interface. Here, TEM is combined with live-cell imaging and electron tomography to reveal the close proximity of endocytic machinery that is shared or distinct to the two pathways. Our focus is the endocytic route(s) taken by antigen-stimulated FcεRI in rat basophilic leukemia cells. We show that FcεRI signaling patches are bordered by distinct topographic features, including multiple coated pits and Arf6-positive structures that appear to be dome-shaped from the cytoplasmic view. These structures are often abutted or connected through membrane projections. Expression of dominant-negative dynamin blocks FcεRI internalization

Journal of Cell Science

through both clathrin-dependent and -independent pathways, consistent with strong dynamin labeling of both Arf6 and clathrin invaginations. The multi-functional adaptor protein Eps15 is found on novel tubule-like membrane structures, as well as being partially colocalized with receptors and Arf6. The marked curvature of membrane labeled for Arf6 and Eps15 suggests that these topographical features might represent a reservoir of lipids and other components needed for endocytic budding.

Results

FcεRI is internalized through clathrin-dependent and -independent pathways

RBL-2H3 ('RBL') cells are derived from rat leukemia cells and retain many characteristics of mucosal mast cells, including surface expression of 200,000–300,000 FcεRI molecules. *In vivo*, FcεRI typically exists in a stable complex with allergen or pathogen-specific IgE acquired from circulating immunoglobulin pools. Here, cultured RBL cells were pre-incubated for 2–24 hours with either unconjugated or fluorescent monoclonal anti-dinitrophenol (DNP) IgE, followed by buffer exchange. Endocytosis of the IgE–FcεRI complex was stimulated by crosslinking with polyvalent antigen (DNP–BSA or DNP–colloidal-gold) (Fattakhova et al., 2006; Molfetta et al., 2009; Wilson et al., 2000; Xue et al., 2007).

Fig. 1A illustrates the remarkable redistribution of crosslinked FcεRI into dark regions of membrane (Wilson et al., 2000) that are typically bordered by clathrin-coated vesicles (arrows). For over a decade, we have noted that these sites often contain multiple buds in various stages of vesicle formation, ranging from flat clathrin arrays to mature vesicles ready for fission. When cells are stimulated by DNP–gold, the nanoparticles are often found in coated vesicles (Fig. 1B), providing solid evidence for FcεRI entry into coated pits.

Despite our own repeated observations of FcεRI in coated pits, Fattakhova and colleagues (Fattakhova et al., 2006) challenged the role of the clathrin pathway in the uptake of IgE receptors by using siRNA methods to knockdown clathrin and adaptor protein 2 (AP2). To evaluate the relative importance of the CME pathway to antigen-stimulated FcεRI internalization, we compared colocalization of fluorescent IgE–FcεRI with GFP–clathrin (Fig. 1C,D), to that of Alexa Fluor 555 (AF555)-tagged transferrin with GFP–clathrin. These live-cell imaging experiments were performed at 16℃ to slow endocytosis and improve the chances of capturing coincidence between GFP–clathrin and IgE–AF555. These representative images show examples of clathin–FcεRI colocalization (yellow arrows, Fig. 1D), as well as examples of clear separation of clathrin and FcεRI in antigen-stimulated cells (Fig. 1C,D, red and green arrows). The plot in Fig. 1E shows a statistical evaluation of IgE and clathrin colocalization (Pearson's coefficient $R=0.33$), as well as transferrin and clathrin ($R=0.53$). Although the colocalization of FcεRI with clathrin is less robust than of transferrin, the combined results of EM and live-cell imaging are consistent with at least partial utilization of the CME pathway.

RNA silencing methods were next used to achieve >90% knockdown of clathrin heavy chain (CHC) (4 days siRNA; Fig. 1F). We combined live-cell imaging and flow cytometric assays (Fig. 1G–I) to evaluate the impact of CHC knockdown on FcεRI internalization. Controls are shown in Fig. 1G, where the *z*-stack composite illustrates the typical punctate intracellular distribution of receptors internalized from the cell surface of antigen-stimulated RBL cells; red vesicles mark the uptake of AF555–transferrin and green vesicles mark endocytosed Alexa Fluor 488 (AF488)-tagged IgE–FcεRI. As shown in supplementary material Movie 1, both red and green fluorescent puncta decorate the cell interior; yellow spots indicate endosomal vesicles containing both cargos. By comparison, the *z*-stack composite image in Fig. 1H (and the associated supplementary material Movie 2) shows that transferrin uptake, but not FcεRI, was blocked after siRNA-mediated CHC knockdown. Fig. 1I reports results of a flow cytometry assay for FcεRI internalization, based upon an acid-stripping protocol to remove surface-exposed IgE. These data show that the kinetics of receptor uptake are unchanged after CHC knockdown. Taken together, Fig. 1G–I demonstrate that crosslinked FcεRI can efficiently take an alternative route for endocytosis if the clathrin pathway is blocked.

We note that additional features are often associated with borders of FcεRI signaling patches, indicated by dotted red outlines in Fig. 1A. Given that these structures lack the honeycomb structure typical of clathrin assemblies and contain abundant gold-labeled FcεRI, we hypothesized that they represent alternative endocytic carriers.

Arf6 is required for FcεRI endocytosis

The small GTPase Arf6 is localized to endosomes (as shown by immuno-labeling of ultrathin sections; Peters et al., 1995), and it is implicated in multiple processes associated with receptor endocytosis and recycling (Donaldson, 2003; Donaldson and Radhakrishna, 2001). To test the possibility that Arf6 is directly or indirectly involved in FcεRI endocytosis, RBL cells were transiently transfected with either wild-type Arf6–GFP or a constitutively active, fluorescent form of Arf6 (Arf6-Q67L–CFP). Surface FcεRI was loaded with IgE–AF555, crosslinked with polyvalent antigen (DNP24–BSA) and incubated for various intervals at 37℃. At the end of the incubation period, cells were rapidly chilled, transferred into ice-cold acidic buffer, to strip IgE–AF555 from any FcεRI remaining on the cell surface, and imaged by confocal microscopy. Results in Fig. 2A,B show that cells expressing Arf6-Q67L–CFP (cyan arrow, Fig. 2B) had markedly diminished uptake of IgE–FcεRI (red arrows, Fig. 2A; supplementary material Fig. S1D) by comparison to untransfected cells (white arrow, Fig. 2B). Control experiments shown in the supplemental material demonstrated that IgE binding in cells expressing wild-type or mutant Arf6–CFP was not altered (supplementary material Fig. S1A,B), and also confirm that antigen-stimulated FcεRI uptake was normal in cells with elevated levels of wild-type Arf6 (transfected with wild-type Arf6–CFP) (supplementary material Fig. S1C).

We next sought insight into the role of Arf6 at the plasma membrane by TEM imaging of immunogold-labeled membrane sheets prepared from transfected cells (Fig. 2C–F; supplementary material Fig. S2A,B). Results showed that Arf6 was markedly enriched in roughly circular structures, often 200–400 nm in diameter. The Ripley's bivariate statistical test was applied to confirm colocalization of anti-GFP 6-nm gold (labeling Arf6) and 10-nm-ligand-coated gold bound to FcεRIβ (Fig. 2G–J).

We note that Arf6-labeled structures are often connected by bridge-like structures to coated vesicles (arrow, Fig. 2E) or occasionally encompass or border clathrin-coated membrane (arrows, Fig. 2F and supplementary material Fig. S2C,D). In order to determine whether the close association between Arf6-positive

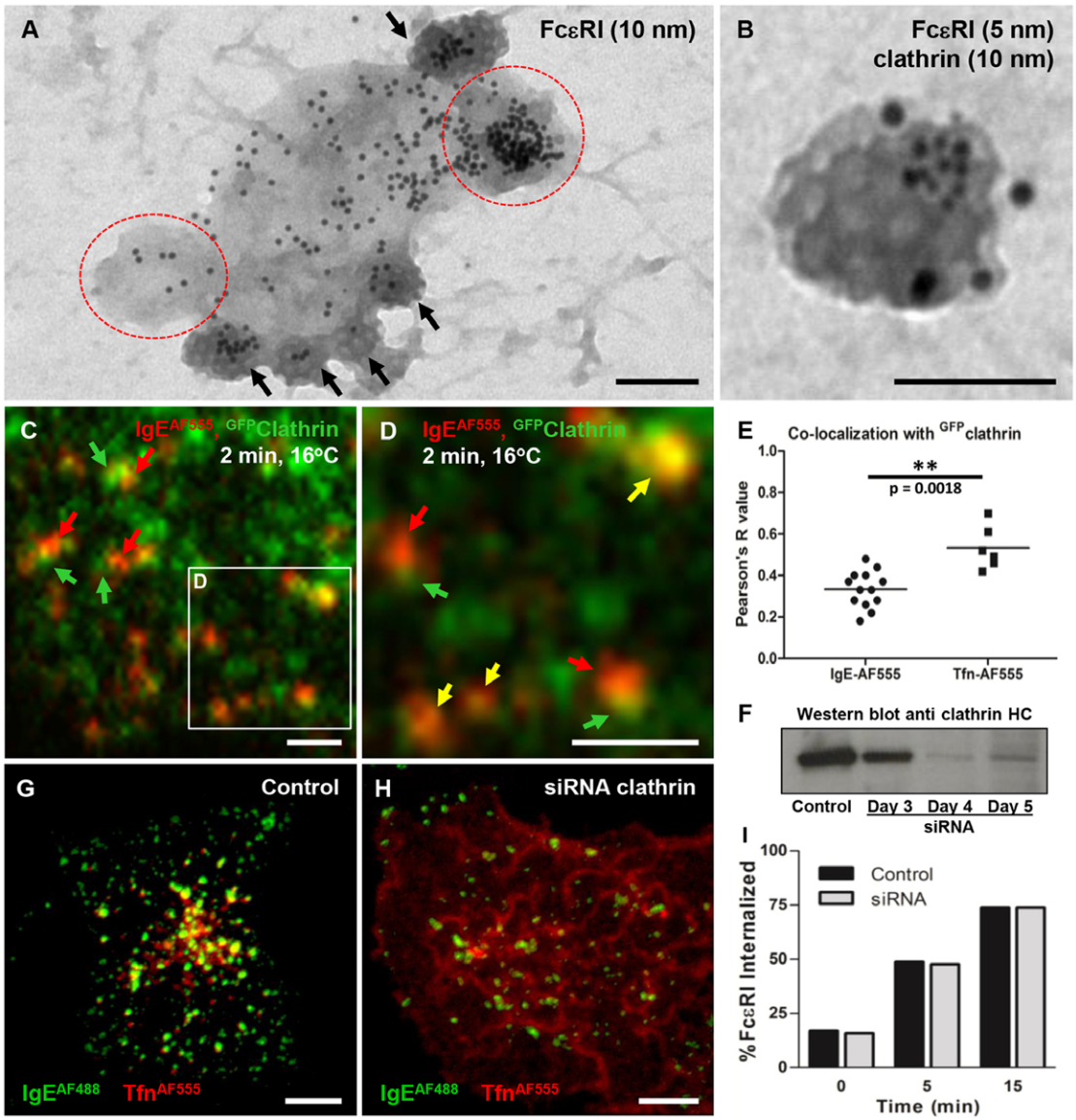

Fig. 1. FcεRI is internalized through clathrin-dependent and -independent pathways. (A,B) TEM image of a membrane sheet prepared from RBL-2H3 cells primed with IgE, and stimulated for 3 minutes with DNP-gold with (B) or without (A) clathrin immunolabeling. (C,D) RBL cells stably expressing GFP–clathrin were primed with IgE–AF555 and then stimulated with DNP24–BSA for 2 minutes at 16℃. Green arrows indicate clathrin punctate, red arrows indicate aggregated FcεRI and yellow arrows indicate colocalization of GFP–clathrin with FcεRI. (E) Quantification of colocalized FcεRI (after DNP24–BSA stimulation) and transferrin with GFP–clathrin. (G,H) Maximum intensity projections of confocal *z*-stacks obtained from cells treated (G) or not (H) with anti-clathrin HC siRNA were primed with IgE–AF488 and then stimulated with DNP24–BSA plus Tfn–AF555 for 10 minutes at 37℃. (F) Western blot showing clathrin HC knockdown with anti-clathrin siRNA over 3–5 days. (I) Internalization assay of FcεRI by flow cytometry on cells treated or not with anti-clathrin siRNA. Cells were primed with fluorescent IgE and stimulated with DNP24–BSA. Endocytosis was measured by flow cytometry using acid stripping to distinguish the fraction of surface versus internalized receptors. Scale bars: 100 nm (A), 50 nm (B), 1 µm (C,D,G,H).

structures and clathrin is dependent on receptor activation, we scored over 600 similar features in resting and antigen-treated cells. Results are summarized in supplementary material Fig. S2E; almost 40% of Arf6 structures were in close proximity to clathrin in resting cells, increasing to ~60% in antigen-stimulated cells.

On the basis of the expectation that membrane features mediating CIE should be invaginated, EM grids bearing immunogold-labeled Arf6 membranes were next examined by electron tomography. Fig. 3 provides 3D reconstructions of Arf6-positive structures from resting cells (Fig. 3B,C) and antigen-stimulated cells (Fig. 3E,F,H,I; supplementary material Movies 3,4); aspects are from the top (Fig. 3B,E,H), at a 30° angle (Fig. 3C,F,I) or side (Fig. 3K). The corresponding 2D TEM image is shown on the left for all three reconstructions (Fig. 3A,D,G). Locations of gold nanoparticles in these images are represented by red spheres. Arrows point to clathrin-coated membrane near or within these structures.

These images provide the first 3D views of Arf6 structures as seen from the cytoplasmic face of the plasma membrane. Remarkably, they show that Arf6 structures can appear as full domes (Fig. 3A–F) or as ‘donuts’ (Fig. 3G–I). At present, we

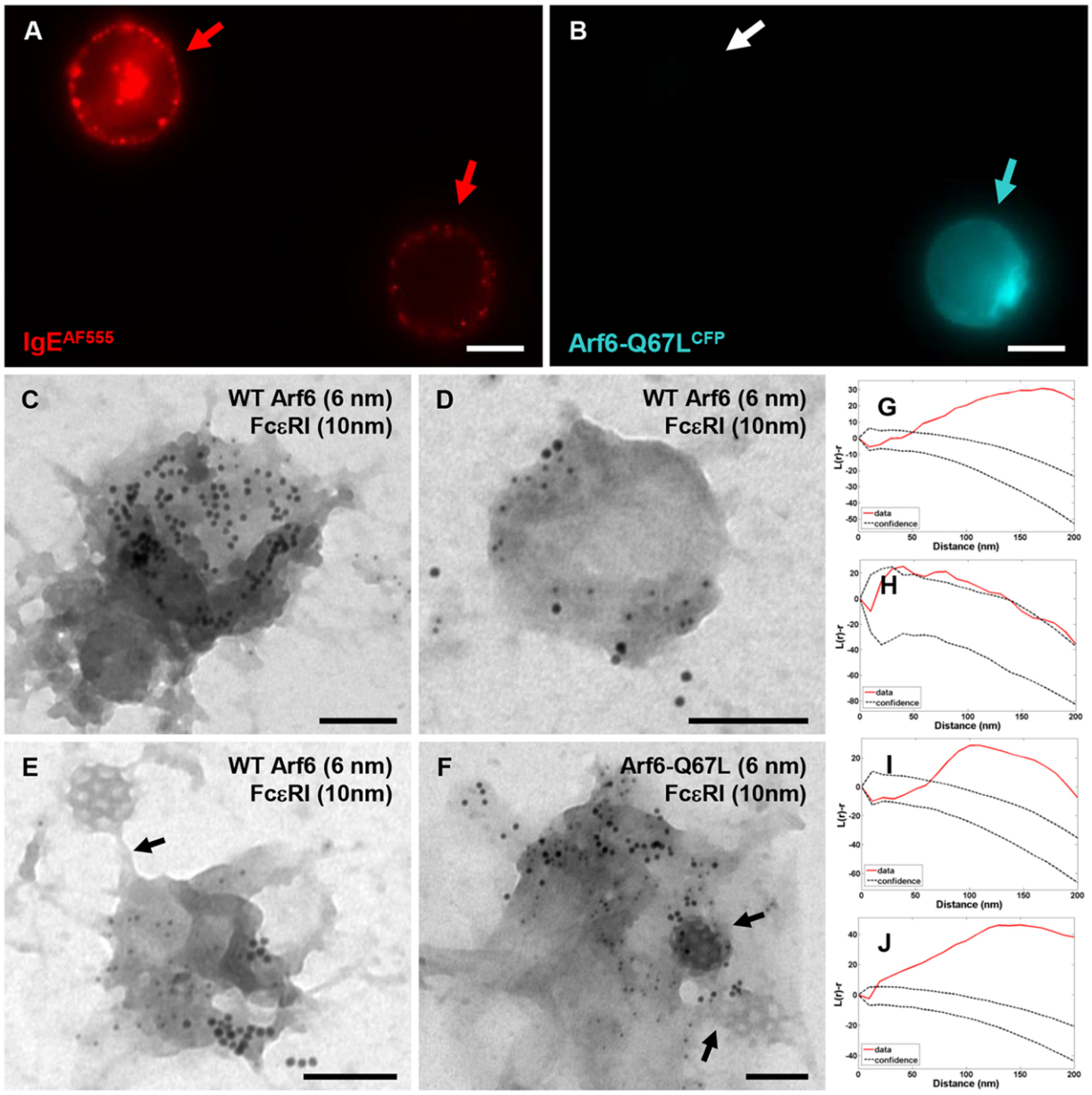

Fig. 2. Arf6 is required for FcεRI endocytosis. (A,B) RBL cells transiently transfected with Arf6-Q67L–CFP were primed with IgE–AF555 and then stimulated with DNP24–BSA for 10 minutes at 37℃. Remaining surface IgE–AF555 was then removed by acid stripping prior to fixation with PFA and imaging. (C–F) TEM images of membrane sheets prepared from cells expressing WT (C–E) or Q67L (F) Arf6 (6 nm gold). Samples were primed with IgE and stimulated for 3minutes with DNP-gold (10 nm gold). (G–J) Ripley's bivariate statistical co-clustering test corresponding to images shown in C–F, respectively. Scale bars: 10 µm (A,B), 100 nm (C–F).

cannot distinguish between the possibility that the donut-like features indicate an intermediate structure associated with the CIE process or the alternative possibility that they represent domes whose center has collapsed during sample preparation. Importantly, analysis of multiple Arf6-positive structures revealed that the height of these structures ranged from 150–300 nm (averaging ~200 nm), with a curvature index of ~0.0025 (Fig. 3J).

Dynamin as a critical player for FcεRI endocytosis

Dynamin facilitates the final stages of vesicle formation, by acting as a 'pinch-ase' during the fission step (Schmid and Frolov, 2011) and was previously implicated in FcεRI endocytosis (Fattakhova et al., 2006). Data in Fig. 4A confirm that the transient expression of dominant-negative dynamin (DYN-K44A), but not expression of wild-type dynamin (WT DYN), blocks the antigen-stimulated uptake of fluorescent IgE as measured by flow cytometry of acid-stripped RBL cells. Electron micrographs in Fig. 4B,E show the relative distribution of wild-type dynamin with respect to labels for FcεRI and clathrin.

We point out that there is strong dynamin labeling at the periphery of coated pits, a view that is uniquely possible in the rip-flip method, consistent with prior reports (Damke et al., 1994; Sundborger et al., 2011) (see supplementary material Movie 5). It suggests that dynamin recruitment to the edges of forming

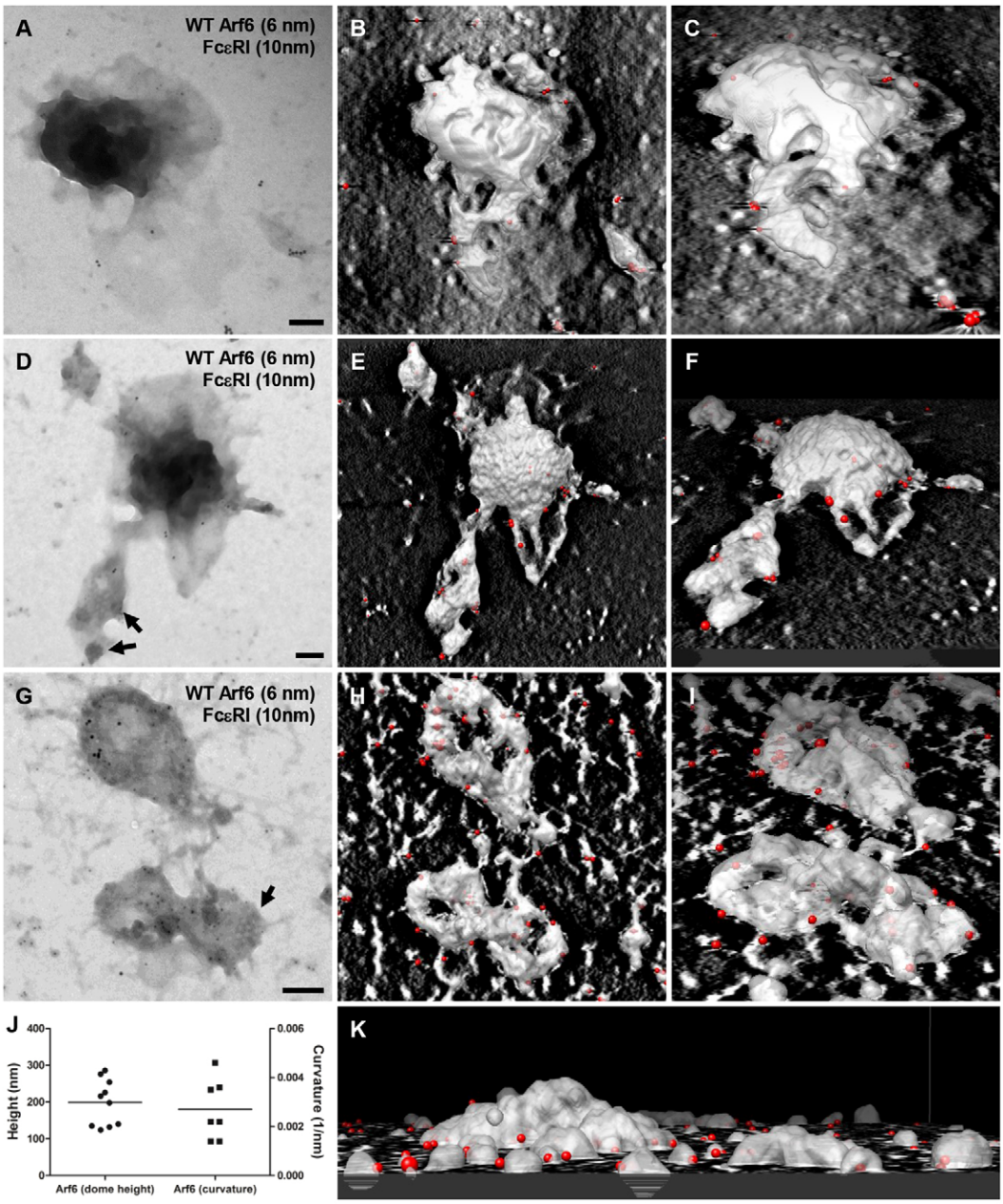

Fig. 3. 2D TEM images and 3D reconstructions of Arf6 endocytic structures. (A,D,G) TEM images of a membrane sheet from RBL cells transiently transfected with WT Arf6 (6 nm gold), primed with IgE (A) and then stimulated with DNP-gold (10 nm gold) for 2minutes at 37°C (D,G). (B,C,E,F,H,I,K) 3D reconstructions of the same structures observed in TEM images shown on the left, based upon EM tomography. WT Arf6 (6 nm gold) and FcεRI (10 nm gold). (J) Plot summarizes the height and curvature of Arf6-positive structures. Scale bars: 100 nm.

vesicles is a step that precedes the assembly of the dynamin 'collars' described by others (McMahon and Boucrot, 2011). These dynamin-labeled peripheral projections are particularly dramatic features of coated pits and flat arrays in cells whose endocytosis is stalled by expression of DYN-K44A–CFP (Fig. 4C,D). Consistent with these observations, cells stably expressing DYN-K44A–eGFP show an accumulation of dynamin puncta at the cell surface (supplementary material Movie 7) in comparison to cells stably expressing wild-type DYN–eGFP (supplementary material Movie 6). In addition, dynamin and FcεRI labeling was observed together in irregular round membrane structures. Colocalization in these features was confirmed using the Ripley's test for FcεRI with both wild-type and mutant dynamin, although the dynamin labeling was typically denser in the cast of the mutant (Fig. 4G,H). Arrows in Fig. 4E,F point to the dynamin gold label that marks projections extending from the edges.

On the basis of the similarity of these round features to Arf6-labeled structures, it seemed likely that they represented the same entity. To address this, we performed both live-cell imaging and triple-labeling TEM experiments. RBL cells were doubly transfected with wild-type monomeric Kusabira orange 2

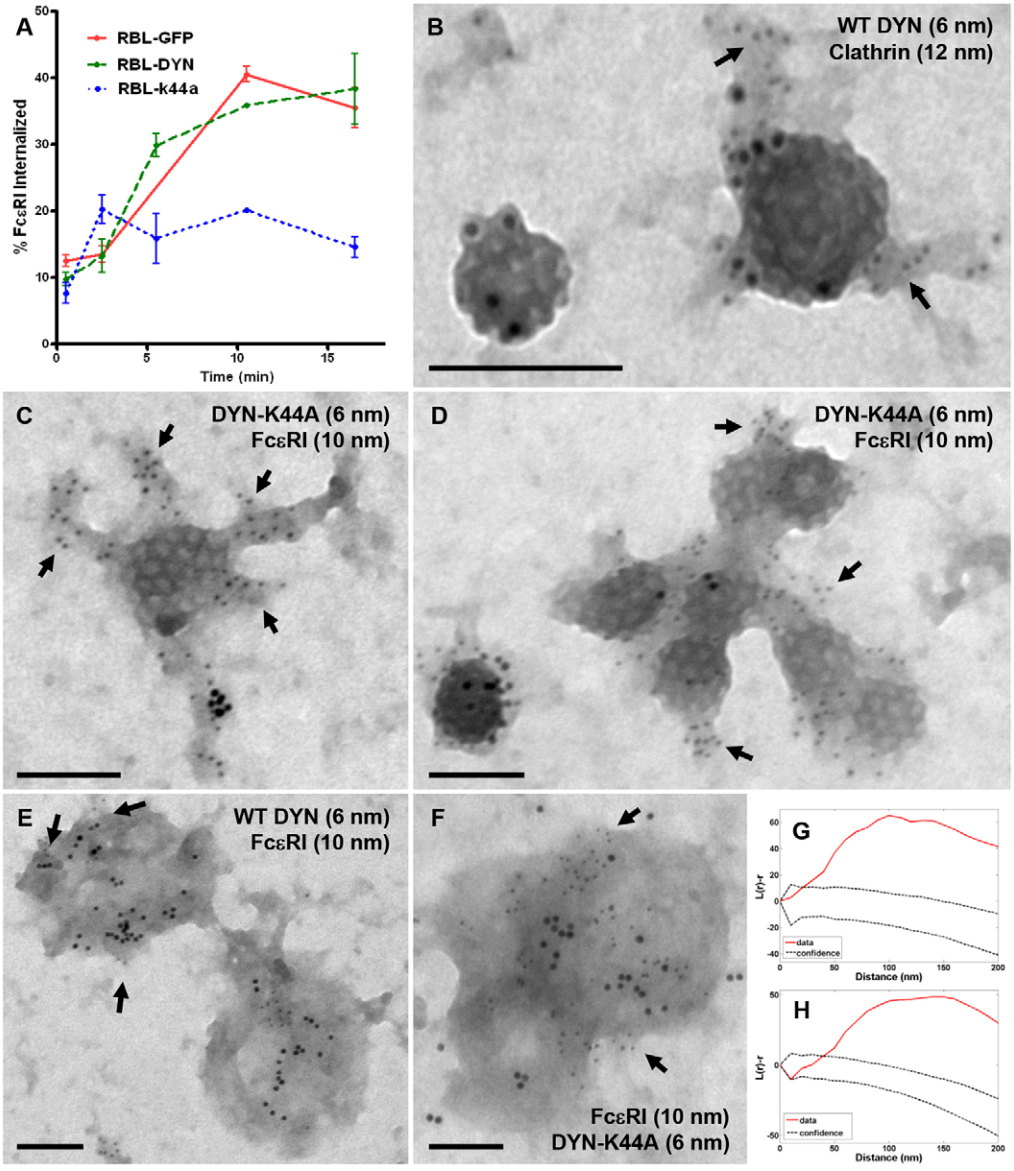

Fig. 4. Dynamin is essential for FcεRI endocytocis. (A) RBL cells transiently transfected with WT or K44A dominant-negative dynamin were primed with IgE–AF488 and then stimulated with DNP24–BSA for 10 minutes at 37℃. Cells were then acid stripped prior to fixation with PFA and the percentage of internalized FcεRI was measured by flow cytometry. (B,F) Electron micrographs of membrane sheets showing 6 nm gold-labeled dynamin WT or K44A, and 10-nm-gold-ligand bound FcεRI after 3 minutes stimulation at 37℃. (G,H) Ripley's bivariate statistical co-clustering test corresponding to the images in E and F, respectively. Scale bars: 100 nm.

(mKO2)-tagged Arf6 and wild-type DYN–eGFP, primed with Pacific Blue 410 (PB410)-tagged IgE, and examined by confocal imaging either before or after crosslinking of FcεRI with DNP24–BSA. Results are shown in Fig. 5. In resting cells (Fig. 5A), both Arf6 and dynamin mostly showed a diffuse distribution. At 2 minutes after stimulation of FcεRI, both Arf6–mKO2 and DYN–eGFP were found in puncta with marked overlap. Even at this early stage of FcεRI aggregation, discrete puncta contain all three fluorescent proteins (IgE–PB410, Arf6–mKO2, DYN–eGFP). By 5 minutes of antigen stimulation, numerous puncta showed overlap (arrowheads in intensity plots). This conclusion was confirmed in membrane sheets labeled for the same three proteins in Fig. 5D,E (FcεRI, blue; Arf6, red; dynamin, green). One notable observation is the concentration of dynamin (green spheres) primarily on the periphery or base. These images strongly suggest that these highly invaginated structures are linked to the clathrin-independent internalization of FcεRI.

Eps15 – a required adaptor protein for FcεRI internalization through CME and CIE, and a marker for highly curved membranes

We next focused on additional strategies to differentiate between clathrin-mediated and clathrin-independent endocytic pathways in mast cells. On the basis of work by Paolini and colleagues (Molfetta et al., 2009) implicating the Eps family of proteins in IgE receptor endocytosis, we double-labeled membrane sheets from activated mast cells for FcεRI and the endocytic adaptor protein, Eps15. Rip-flips were prepared after 2–5 minutes of exposure to antigen. Results were striking, showing several distinct patterns: (1) densely labeled Eps15 membrane adjacent to, but poorly mixed with, clustered FcεRI (Fig. 6A,B and supplementary material Fig. S3F,G); or (2) coincident labeling of FcεRI, Eps15 and Arf6 on both dome-like (Fig. 6C and supplementary material Fig. S3K) and tubular (supplementary material Fig. S3I–J) structures. Tubular Eps15 structures were striking features on RBL membranes (Fig. 6D). Like Arf6,

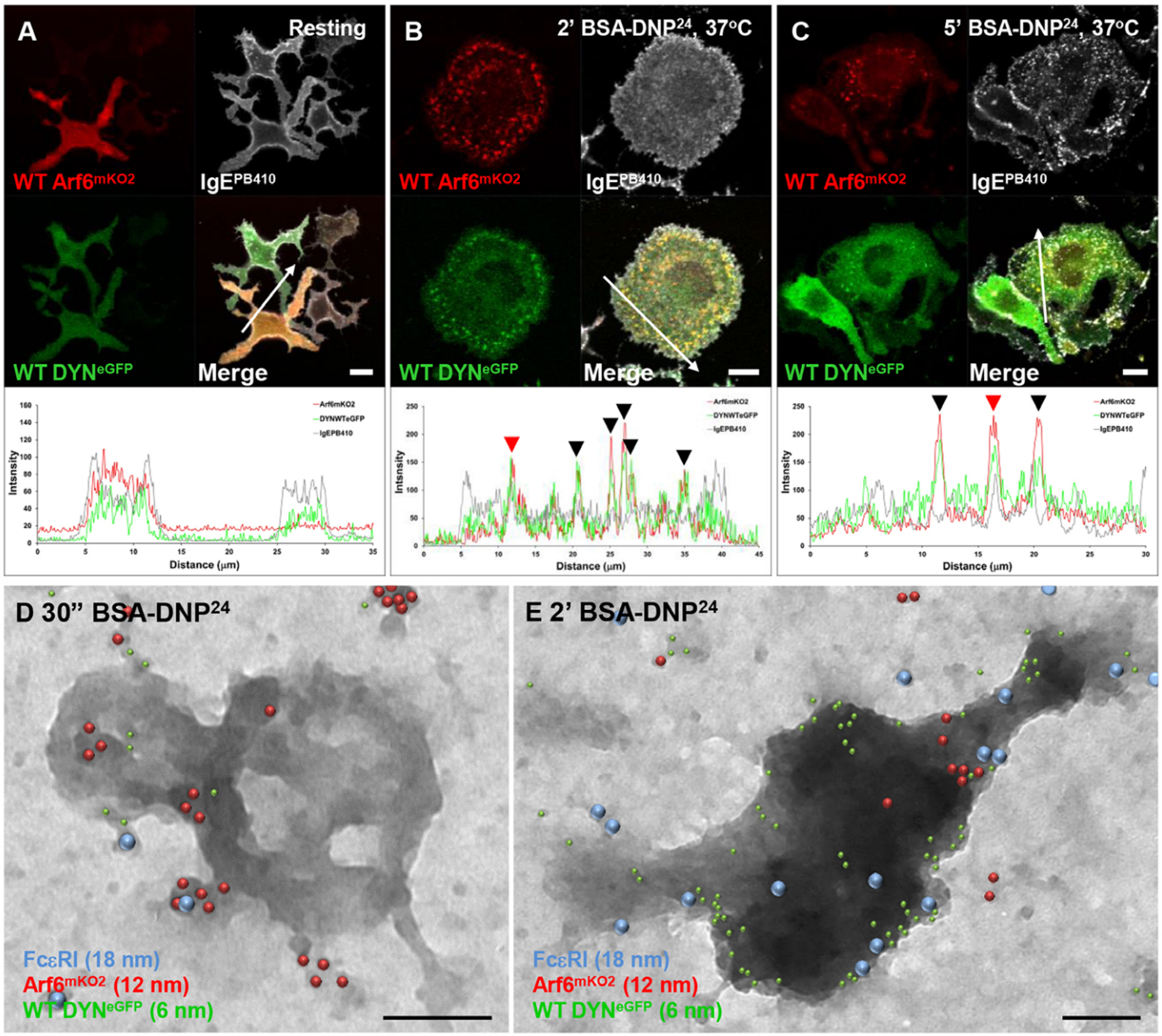

Fig. 5. Arf6 and dynamin colocalize upon FcεRI crosslinking. Confocal images of RBL cells doubly transfected with Arf6–mKO2 and dynamin–eGFP primed with IgE–PB410 in the resting state (A) or cross-linked for 2 minutes (B) or 5 minutes (C). Profiles of fluorescence (across individual cells and indicated by a white arrow) show that there is a good colocalization of Arf6–mKO2 and dynamin–eGFP in RBL cells, with (red arrowheads) or without (black arrowheads) the IgE receptor. (D,E) Electron micrographs of membrane sheets triply labeled for WT DYN–eGFP (6 nm gold, green dots), Arf6–mKO2 (12 nm gold, red dots) and FcεRIβ (18 nm gold, blue dots) after 30 seconds (D) or 2 minutes (E) stimulation at 37°C. Scale bars: 10 μm (A–C), 100 nm (D,E).

Eps15-labeled structures are often adjacent to coated pits (Fig. 6A,B; supplementary material S3H,J).

IgE receptor internalization was next evaluated in cells transfected with either wild-type or dominant-negative Eps15–eGFP fusion proteins (WT Eps15–eGFP or Eps15-DIII–eGFP, respectively). A null version (Eps15-D3Δ2–eGFP) served as a negative control. Results are reported in the Fig. 6I–K and in supplementary material Fig. S3D–F. We found that wild-type Eps15–eGFP overexpression resulted in accumulation of bright fluorescent objects at the cell periphery (green, Fig. 6I). These punctate structures remain in contact with the plasma membrane, based upon confocal *z*-stack reconstructions (supplementary material Movie 8). Uptake of both receptors was normal in cells expressing either wild-type Eps15 (Fig. 6I), or the null version (Eps15-D3Δ2; supplementary material Fig. S3A,C). Expression of Eps15-DIII–eGFP dramatically blocked transferrin uptake and partially blocked antigen-stimulated FcεRI internalization (Fig. 6J). Partial block of FcεRI internalization is consistent with previously published results showing that triple knockdown of Eps15, Eps15R and epsin are required to ablate FcεRI endocytosis (Molfetta et al., 2009). We also noted a large increase in the incidence of flat clathrin arrays on membranes prepared from cells

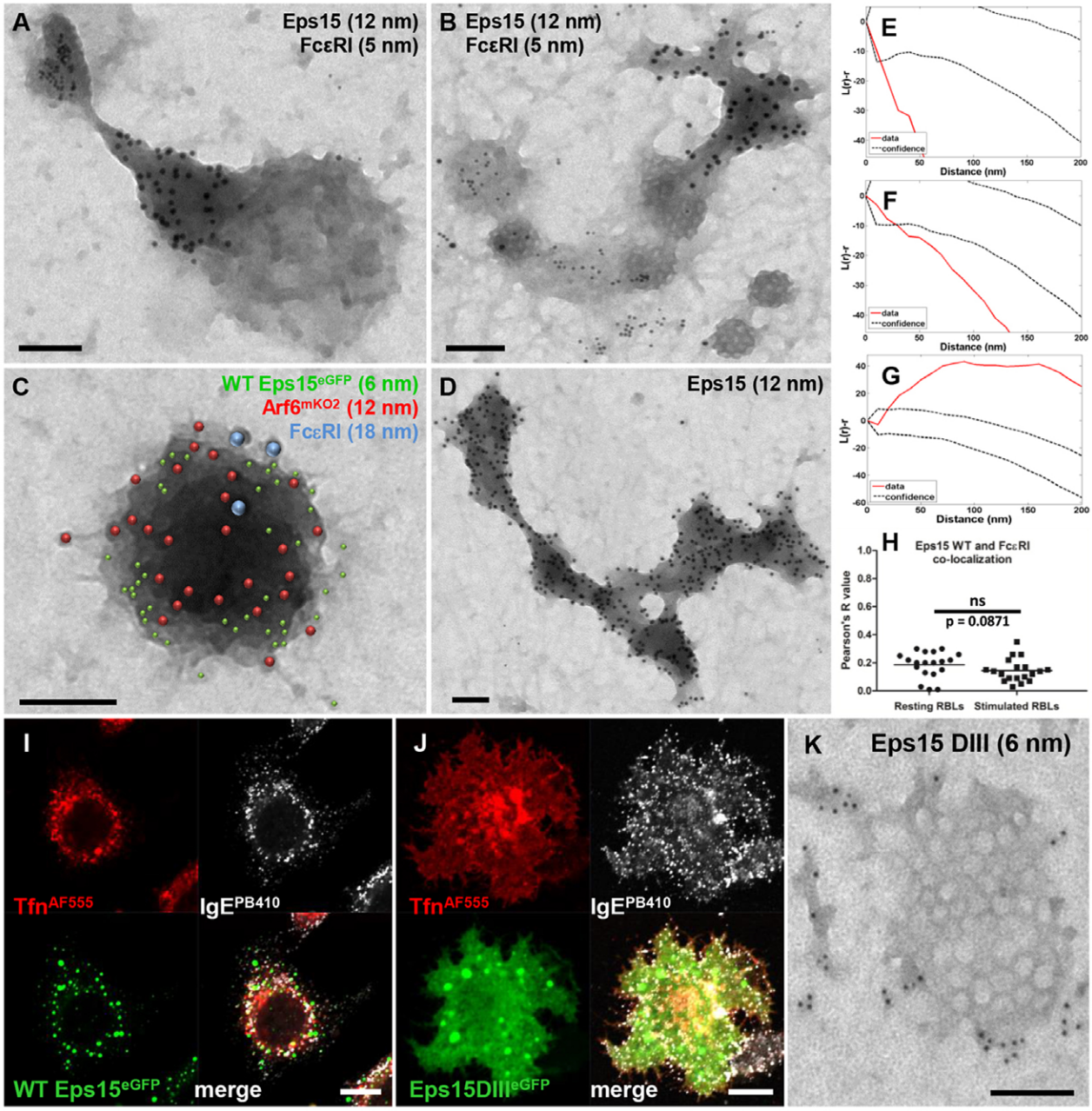

Fig. 6. Eps15 is essential for CME and CIE. (A,B,D) Electron micrographs showing Eps15 (12 nm gold) and FcεRI (5 nm gold) on membrane sheets obtained from RBL cells primed with IgE in the resting condition (D) or stimulated with DNP-gold for 5 minutes at 37℃ (A,B). (C) Electron micrographs of membrane sheets triply labeled for WT Eps15–eGFP (6 nm gold, green dots), Arf6–mKO2 (12 nm gold, red dots) and FcεRIβ (18 nm gold, blue dots) after a 1-minute stimulation at 37℃. (E–G) Ripley's bivariate statistical co-clustering tests for Eps15 and FcεRI (E,F), or Eps15 and Arf6 (G), corresponding to the images in A–C, respectively. (H) Pearson's correlation plot for colocalization of WT Eps15 and FcεRI in the resting or antigen-stimulated condition. (I,J) Confocal image of RBL cells transiently transfected with WT Eps15–eGFP (I) or the dominant-negative Eps15-DIII–eGFP (J) primed with IgE–PB410 and stimulated with DNP24 and Tfn–AF555 for 10 minutes at 37℃. (K) Electron micrograph of RBL-2H3 cells expressing Eps15-DIII–eGFP (6 nm gold). Scale bars: 100 nm (A–D,K), 10 μm (I,J).

expressing the dominant-negative Eps15 mutant (Fig. 6K; supplementary material Fig. S3D,E).

We do not yet know the identity or function of these pools of Eps15. We speculate that they represent nucleation sites where Eps15 and associated F-BAR proteins associate with specific lipids needed to form invagination cups for one – or perhaps both – internalization pathways. Consistent with this intriguing notion, the 3D tomographic reconstructions show that heavily labeled Eps15 structures are highly curved (Fig. 7; supplementary material Movie 9,10). They extend inwardly to almost the same degree as Arf6-positive structures, with a maximum height of 200 nm (Fig. 7G) and a curvature index of up to 0.0028 per nm.

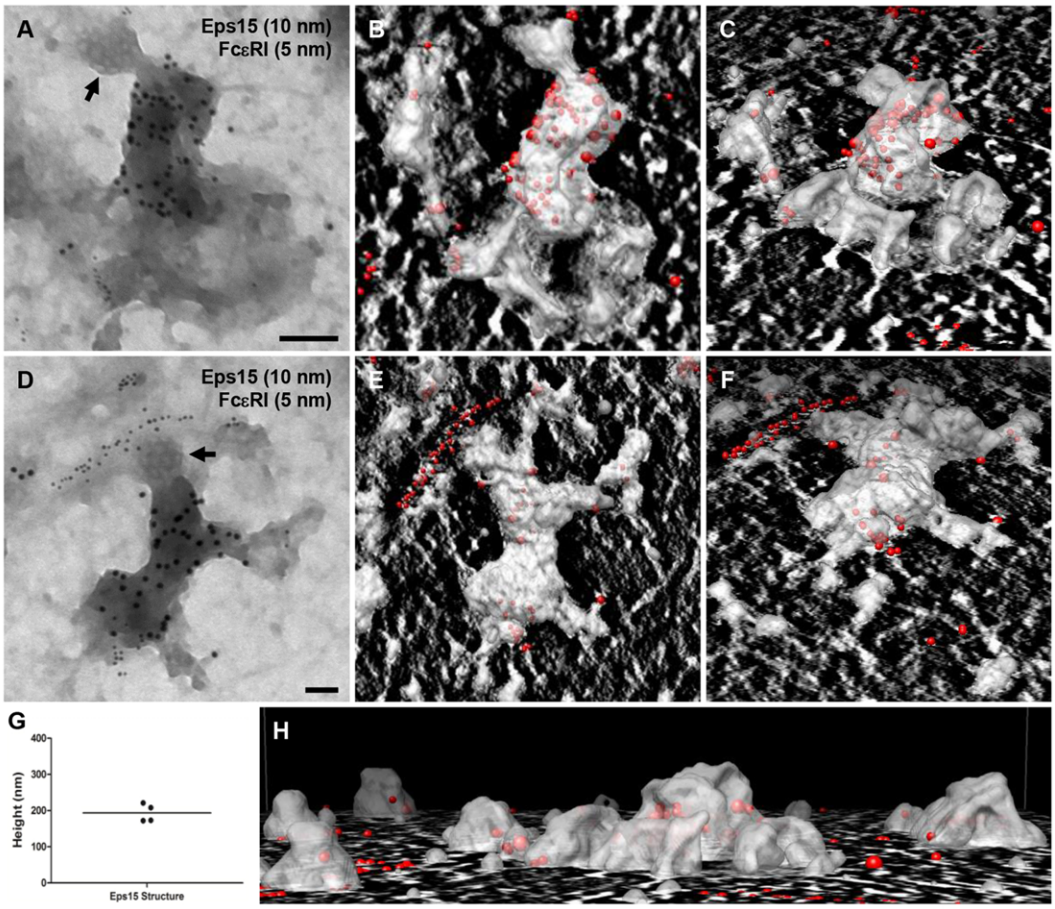

Fig. 7. 2D TEM images and 3D reconstructions of Eps15 structures. (A,D) TEM images of a membrane sheet from RBL-2H3 cells labeled with an anti-Eps15 antibody (10 nm gold), primed with IgE and then stimulated with DNP-gold (5 nm gold) for 10 minutes at 37℃. (B,C,E,F,H) 3D reconstructions of the same structures observed in the TEM images shown in A and B, based upon EM tomography. (G) Plot summarizes height of Eps15 positive structures. WT Eps15 (10 nm gold) and FcεRI (5 nm gold). Scale bars: 100 nm.

Pitstop2 blocks CME and CIE in mast cells

Our evidence for spatial relationships between Arf6, Eps15 and clathrin structures suggest that FcεRI signaling patches represent 'sorting stations' for internalization by the two complimentary pathways. To investigate further the relationship between these endocytosis pathways, we evaluated the ability to block receptor uptake with the inhibitor Pitstop2 (von Kleist et al., 2011). This compound was originally described as a specific CME inhibitor, based upon its direct association with clathrin terminal domain (TD) and on *in vitro* evidence that it inhibits formation of the complex between the clathrin TD and amphiphysin. A recent article by Donaldson and colleagues indicates that Pitstop2 also blocks CIE, raising the possibility that this drug has other common or distinct targets in the endosome sorting process (Dutta et al., 2012).

Given that the original characterization of Pitstop2 was performed in HeLa cells, we first established conditions for blocking of transferrin internalization in these cells (60 μM Pitstop2; Fig. 8A–C). In RBL cells, 30 μM Pitstop markedly diminished both transferrin and IgE–FcεRI uptake (Fig. 8E) with essentially a complete block of internalization for both receptors at 60 μM (Fig. 8F). Fig. 8G–I show *z*-stack reconstructions of fluorescent IgE-labeled FcεRI puncta in control (Fig. 8G) and Pitstop2-treated cells (Fig. 8H,I). Supplementary material movies 11,12 show that FcεRI aggregates are internalized within minutes after antigen-mediated crosslinking in control cells. These aggregates are largely trapped on the cell surface when cells are pre-treated with Pitstop2 before antigen addition.

Discussion

Upon aggregation by IgE and polyvalent antigens, FcεRI redistributes to distinctive plasma membrane 'signaling patches' that recruit tyrosine kinases, adaptor proteins and other components to propagate the signaling cascade (Wilson et al., 2000; Wilson et al., 2001; Wilson et al., 2004). By documenting that the signaling-competent FcεRI is also spatially related to key proteins controlling both clathrin-mediated and clathrin-independent endocytosis pathways, we infer that the signaling patches are also the locations for sorting of FcεRI into endocytic carriers. This is a critical connection because the duration of signaling at the plasma membrane is directly linked to the rate at which receptors are internalized. We also confirm that FcεRI endocytosis by both routes is dependent upon dynamin (Fattakhova et al., 2006) and show that, although the CME pathway can be utilized by aggregated FcεRI, it is unlikely to be the major route. FcεRI internalization is blocked by Pitstop2, a reagent that has been recently shown to affect both pathways (Dutta et al., 2012; Lemmon and Traub, 2012).

What triggers the internalization of FcεRI and other closely related immunoreceptors? On the basis of the mutagenesis studies of Metzger and colleagues, FcεRI cytoplasmic tails lack specific endocytic sorting signals (Mao et al., 1993; Mao et al., 1991). Instead, the extent of aggregation is the key criteria regulating the internalization of FcεRI (Andrews et al., 2009). This is a feature shared with glycolipids, such as gangliosides and glycosphingolipids, whose endocytosis by several routes can be

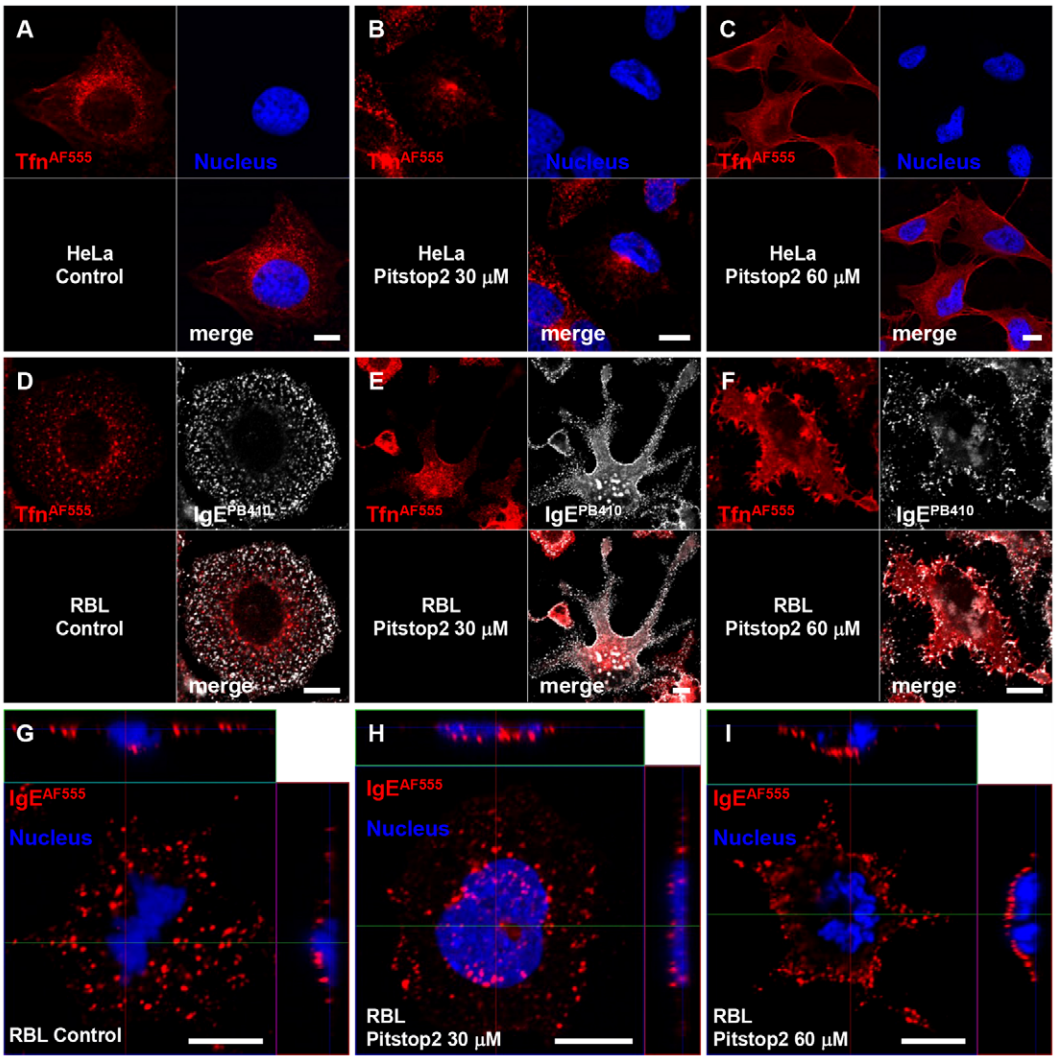

Fig. 8. Pitstop2 blocks CME and disturbs CIE of FcεRI. (A–C) HeLa cells, used as a control cell line, were stimulated with Tfn–AF555 in the absence (A) or the presence of Pitstop2 at 30 μM (B) or 60 μM (C). Transferrin uptake is blocked when using Pitstop2 at 60 μM. (C). (D–F) Images of RBL cells primed with IgE–PB410 and stimulated with DNP24 for 10 minutes at 37℃ in the presence of Tfn–AF555 and with 30 μM Pitstop2 (E), 60 μM Pitstop2 (F) or without Pitstop2 (D), showing that the uptake of both the transferrin and the IgE receptors is blocked. (G–I) *z*-stack orthogonal views of RBL cells primed with IgE–AF555 and crosslinked with DNP24–BSA for 10 minutes at 37℃, without (G) or with at 30 μM (H) or 60 μM (I) Pitstop2 treatment. Nuclei are counterstained with Hoechst 33258 (blue). Scale bars: 10 μm.

activated by crosslinking (Oliver et al., 2007; Torgersen et al., 2001). Linked to aggregation state is the recruitment of ubiquitin ligases, such as Cbl (Wilson et al., 2002), that catalyze ubiquitylation of receptors and/or associated cytosolic partners. Subsequent steps in the process include recruitment of ubiquitin-binding proteins that serve both distinct and overlapping functions for both CME and CIE pathways. (Hurley and Wendland, 2002; Paolini and Kinet, 1993; van Bergen en Henegouwen, 2009). Parallels can be found in the epidermal growth factor receptor literature. For example, Sigismund et al. (Sigismund et al., 2005) proposed that Cbl-mediated ubiquitylation of clathrin-associated endocytic machinery is favored at low ligand doses of EGF, whereas ubiquitylation of EGFR itself is substantial only at high ligand doses where endocytosis ‘switches’ to a non-clathrin pathway.

Consistent with ubiquitylation being a driver of FcεRI endocytosis, we found Eps15 to be colocalized with FcεRI (Fig. 6C; supplementary material Fig. S3H–K) as well as in distinctive, highly curved membrane areas near receptor signaling patches (Fig. 6A,B; supplementary material Fig. S3F,G). Eps15 and its family members, Eps15R and Eps15b, are modular proteins that bind mono-ubiquitylated peptides through their UIM domains and are themselves substrates for mono-ubiquitylation (reviewed in Polo, 2012). Their EH domains interact with other EH domain proteins (EHDs), multiple adaptors (Epsin1, STAM, Stonin2, Numb, synaptojanin) and phosphatidylinositols (reviewed in van Bergen en Henegouwen, 2009), whereas their coiled-coil domains mediate oligomerization and capture cargo (Parachoniak and Park, 2009). Their DPF motifs permit association with adaptins of

AP1 and AP2 complexes (van Bergen en Henegouwen, 2009). Molfetta and colleagues showed that triple knockdown of Eps15, Eps15R and epsin is needed to ablate FcεRI internalization (Molfetta et al., 2009), which suggests there is partial overlap of their function. Because of heavy Eps15 labeling of tubules near clathrin pits and partial colocalization with Arf6, we speculate that Eps15 and related proteins provide a reservoir of curved bilayer available to enhance endocytic budding efficiency for both CME and CIE pathways. This concept is consistent with results in cells expressing the dominant-negative form of Eps15 (Eps15DIII–eGFP), where there is a preponderance of flat clathrin arrays and a block in FcεRI uptake (Fig. 6J,K; supplementary material Fig. S3D,E).

Arf6, shown here to be required for FcεRI endocytosis, might be exerting its control through local lipid remodeling. The characteristic dome-like regions that label heavily for Arf6 could be hot spots for the activity of its effectors, phospholipase D and phosphatidylinositol 5-kinase, and the production of the lipid products phosphatidic acid and PtdIns(4,5)P_2 (reviewed in (Doherty and McMahon, 2009)). The observation that Arf6-Q67L strongly labels these domes is consistent with prior evidence showing that GTP-loaded Arf6 is capable of inserting its N-terminal amphipathic helix into lipid monolayers, preferentially loading onto (and reinforcing) positive membrane curvature (Pasqualato et al., 2001).

Understanding the complex interplay between lipids and proteins in the regulation of endocytosis might be best approached through modern systems biology analytical methods (Ramanan et al., 2011; Zwang and Yarden, 2009). Here, we point out that these relationships appear to be orchestrated in a spatially integrated manner that requires both mixing and lateral communication. Nossal and Zimmerberg have proposed that ENTH domains in epsin and its relatives can bend membranes by inserting into the inner leaflet (Nossal and Zimmerberg, 2002); epsin is a primary binding partners of Eps15. Once a patch of curved membrane is created, clathrin and other adaptors could move in to provide stability. Even higher degrees of curvature associated with neck constriction have additional requirements, such as dynamin and structurally similar proteins like the EHD ATPases (Daumke et al., 2007). Because Eps15 does not follow cargo into coated vesicles (Cupers et al., 1998), we propose that endocytic vesicles could begin the budding process from the reservoir of curved membrane created by Eps15 and its binding partners. Rather than displacing this critical machinery, they might move laterally in a fluid process that is suggested by the tubular bridges seen in Fig. 6A,B and Fig. 7A,D. Testing of this hypothesis will require sophisticated single-molecule imaging techniques in live cells, where the time-resolved diffusion process can be directly observed. It will be a challenge to capture the dynamics of sorting and lipid remodeling within the confinements of the FcεRI signaling patch, where receptor motion is expected to be severely restricted by diffusion barriers and by adaptor-mediated trapping.

Materials and Methods

Reagents and cell culture

RBL-2H3 and stable transfectants were maintained in MEM (Invitrogen; Carlsbad, CA) supplemented with 10% fetal bovine serum, penicillin-streptomycin and L-glutamine. Affinity purified anti-DNP IgE was prepared in house as described previously (Liu et al., 1980). Fluorescent IgE conjugates were created using N-hydroxysuccinimide esters of chromophores (Invitrogen; Carlsbad, CA). Monoclonal antibodies to anti-clathrin heavy chain were purchased from Calbiochem (San Diego, CA) and anti-GFP antibodies were from Invitrogen. Secondary antibodies were from Jackson Laboratories. Fluorescent transferrin was from Invitrogen. Primary antibodies directed against mKO2 and FcεRIβ were purchased from MBL International Corporation (#PM051) and Santa Cruz Biotechnology, respectively.

siRNA experiments

Anti rat CHC (#E-090659-00-0005) and non-targeting (NT) (#D-001910-10-05) siRNA were purchased from Thermo Scientific. RBL cells were incubated with either anti-CHC or NT siRNA at 1 μM in Accel delivery media (Thermo Scientific) following the manufacturer's recommendations. After 72, 96 and 120 hours, cells were lyzed in RIPA buffer and analyzed by western blotting.

Flow cytometric internalization assay

RBL-2H3 cells were primed in suspension by 2 hour incubation at 37℃ with 2 μg/ml Alexa-Fluor-488 or Alexa-Fluor-555-tagged IgE–DNP in MEM plus 10% FBS. Cells were then pelleted and washed once with HBSS. After washing, cells were stimulated for defined intervals with the indicated doses of DNP–BSA. Samples were then split into two, and one sample for each condition was subjected to a light acid strip by a 10-minute incubation at 4℃ in 0.5 M NaCl and 0.2 M acetic acid (pH 2.7) to remove any surface-accessible fluorescent IgE. All samples were then fixed by a 20-minute incubation in 2% paraformaldehyde at room temperature in PBS, and IgE fluorescence levels were measured by flow cytometry. The ratio of the acid-stripped and non-stripped samples for each condition was then used to calculate the percentage of internalized IgE–FcεRI.

Transient and stable transfection

RBL-2H3 cells were transfected using an Amaxa device (Lonza) following the manufacturer's protocol. Stable transfectants were obtained using the appropriate selective agent. Arf6–CFP-encoding plasmids were from Addgene (no. 11382, no. 11386 and no. 11387) and dynamin–eGFP-encoding plasmids were from Sandra Schmid (Scripps Institute, San Diego, Ca); the design of Eps15–eGFP-encoding plasmids is as described previously (Benmerah et al., 1998). The Arf6–mKO2-encoding plasmid was constructed by gene fusion PCR between wild-type Arf6 and mKO2 and then sub-cloned into the directional topo vector pcDNA 3.1 from Invitrogen.

Fluorescence microscopy

For live-cell microscopy, cell monolayers were cultured in eight-well Lab-Tek chambers (Nunc, Rochester, NY) 24 hours before experiments and primed with IgE–AF488, IgE–AF555 or IgE–PB410. Confocal imaging was performed on a Zeiss LSM 510 META system equipped with a 63× 1.4 N.A. oil objective. For fluorescence studies, cells were cultured on glass coverslips, treated with polyvalent ligand or drugs as described in figure legends, then fixed for 20 minutes in 2% paraformaldehyde. Samples were mounted on slides in Prolong Gold (Invitrogen) anti-fade reagent prior to imaging.

Preparation of plasma membrane sheets, gold labeling for TEM, tomography and image analysis

Membrane sheets were prepared as described (Wilson et al., 2007). In brief, cells were plated on 15-mm round, clean glass coverslips 24 and cultured overnight. After defined periods of incubation at 37℃ with or without stimuli, cells on the coverslips were fixed in 0.5% paraformaldehyde for 7 minutes at room temperature. Coverslips were then immersed in ice-cold HEPES buffer (25 mM HEPES pH 7, 25 mM KCl, 2.5 mM magnesium acetate) and inverted onto dry Formvar and poly-L-lysine-coated nickel electron microscopy grids. Pressure was applied to the coverslip for 20 seconds by bearing down with a cork. The coverslips were lifted, leaving sections of the upper cell surface adherent to the poly-L-lysine-coated grid. Membranes were further fixed in 2% paraformaldehyde (10 minutes at 4℃). After washing, antigens on the cytoplasmic membrane face were labeled by incubating sequentially with primary antibodies and gold-conjugated secondary reagents. Samples were post-fixed with 2% glutaraldehyde for 10 minutes at room temperature, processed for TEM analysis and 2D images were acquired on a Hitachi H7500 transmission electron microscope.

Statistical analysis

Digital TEM images were analyzed with a FIJI (ImageJ) plugin (Particle Picker) customized to find and count coordinates of two sizes of gold particles (Zhang et al., 2006). Ripley's K bivariate function was utilized to evaluate co-clustering using the gold code for MATLAb (Wilson et al., 2004; Zhang et al., 2006). The Pearson's pixel intensity correlation over space coefficients of 2D bi-color confocal images were calculated using the Coloc_2 plugin of FIJI.

Electron tomography and image analysis

Tomographic tilt series (approximately −70 to +70°, every 2°) were acquired on a Tecnai G2 F20 (FEI Company) equipped with an energy filter (zero-loss, Gatan Inc.) using a 2020 advanced tomography holder (Fishione Instruments). The data

was collect using SerialEM (Mastronarde, 2005). Prior to reconstruction, the images were processed for noise reduction and feature enhancement with 150 iterations of curvature anisotropic diffusion (Whitaker and Xue, 2001) as implemented in the CoAn package (Volkmann and Hanein, 1999). 3D reconstructions were generated using alignment and backprojection algorithms implemented in the IMOD package (Kremer et al., 1996). Segmentation of membrane compartments was achieved using the watershed algorithm (Volkmann, 2002) after application of 30× iterative median filtering (van der Heide et al., 2007). The positions of the different sized gold labels were separately extracted using a 3D version of the reduced representation template-matching algorithm (Volkmann, 2004). Surface and volume representations were generated using Chimera (Pettersen et al., 2004). Average curvatures were estimated by fitting an ellipsoid to the surfaces of the protruding domes. Spatial statistics tools used here are available at http://stmc.health.unm.edu/tools-and-data/index.html.

Acknowledgements

Images in this paper were generated in the University of New Mexico & Cancer Center Fluorescence Microscopy Shared Resource, funded as detailed on: http://hsc.unm.edu/crtc/microscopy/acknowledgement.shtml. Flow data were generated in the Flow Cytometry Shared Resource Center supported by the University of New Mexico Health Sciences Center and Cancer Center. For superb technical assistance, we thank Rachel Grattan, Janet Pfeiffer, Angela Welford, Floriant Dingreville, Anna Holmes, Gordon Zwartz and Mary Ann Raymond-Stintz (UNM), as well as Wendy F. Ochoa (Sanford-Burnham). The gift of plasmids from Sandra Schmid (University of Texas Southwestern) and Alexandre Benmerah (Institut Cochin, Université Paris Descartes) is gratefully acknowledged. The authors have no conflicts of interest to report.

Author contributions

C.C. and B.S.W designed experiments and wrote the manuscript. C.C., A.D., K.L.A., C.P., D.S.L., N.V. and D.H. performed experiments and data analysis.

Funding

This work was supported by the National Institutes of Health [grant numbers R01 AI051575, P50 GM065794 to B.S.W.], which supports the NM Spatiotemporal Modeling Center. The electron tomography and image analysis portion of the study was also supported by the National Institutes of Health [grant number P01 GM098412 to D.H. and N.V.]. Deposited in PMC for release after 12 months.

Supplementary material available online at
http://jcs.biologists.org/lookup/suppl/doi:10.1242/jcs.128876/-/DC1

References

Andrews, N. L., Pfeiffer, J. R., Martinez, A. M., Haaland, D. M., Davis, R. W., Kawakami, T., Oliver, J. M., Wilson, B. S. and Lidke, D. S. (2009). Small, mobile FcepsilonRI receptor aggregates are signaling competent. *Immunity* **31**, 469-479.

Benmerah, A., Lamaze, C., Bègue, B., Schmid, S. L., Dautry-Varsat, A. and Cerf-Bensussan, N. (1998). AP-2/Eps15 interaction is required for receptor-mediated endocytosis. *J. Cell Biol.* **140**, 1055-1062.

Chadda, R., Howes, M. T., Plowman, S. J., Hancock, J. F., Parton, R. G. and Mayor, S. (2007). Cholesterol-sensitive Cdc42 activation regulates actin polymerization for endocytosis via the GEEC pathway. *Traffic* **8**, 702-717.

Cupers, P., Jadhav, A. P. and Kirchhausen, T. (1998). Assembly of clathrin coats disrupts the association between Eps15 and AP-2 adaptors. *J. Biol. Chem.* **273**, 1847-1850.

Damke, H., Baba, T., Warnock, D. E. and Schmid, S. L. (1994). Induction of mutant dynamin specifically blocks endocytic coated vesicle formation. *J. Cell Biol.* **127**, 915-934.

Daumke, O., Lundmark, R., Vallis, Y., Martens, S., Butler, P. J. and McMahon, H. T. (2007). Architectural and mechanistic insights into an EHD ATPase involved in membrane remodelling. *Nature* **449**, 923-927.

Doherty, G. J. and McMahon, H. T. (2009). Mechanisms of endocytosis. *Annu. Rev. Biochem.* **78**, 857-902.

Donaldson, J. G. (2003). Multiple roles for Arf6: sorting, structuring, and signaling at the plasma membrane. *J. Biol. Chem.* **278**, 41573-41576.

Donaldson, J. G. and Radhakrishna, H. (2001). Expression and properties of ADP-ribosylation factor (ARF6) in endocytic pathways. *Methods Enzymol.* **329**, 247-256.

Dutta, D., Williamson, C. D., Cole, N. B. and Donaldson, J. G. (2012). Pitstop 2 is a potent inhibitor of clathrin-independent endocytosis. *PLoS ONE* **7**, e45799.

Fattakhova, G., Masilamani, M., Borrego, F., Gilfillan, A. M., Metcalfe, D. D. and Coligan, J. E. (2006). The high-affinity immunoglobulin-E receptor (FcepsilonRI) is endocytosed by an AP-2/clathrin-independent, dynamin-dependent mechanism. *Traffic* **7**, 673-685.

Glebov, O. O., Bright, N. A. and Nichols, B. J. (2006). Flotillin-1 defines a clathrin-independent endocytic pathway in mammalian cells. *Nat. Cell Biol.* **8**, 46-54.

Goh, L. K., Huang, F., Kim, W., Gygi, S. and Sorkin, A. (2010). Multiple mechanisms collectively regulate clathrin-mediated endocytosis of the epidermal growth factor receptor. *J. Cell Biol.* **189**, 871-883.

Hurley, J. H. and Wendland, B. (2002). Endocytosis: driving membranes around the bend. *Cell* **111**, 143-146.

Kirkham, M., Fujita, A., Chadda, R., Nixon, S. J., Kurzchalia, T. V., Sharma, D. K., Pagano, R. E., Hancock, J. F., Mayor, S. and Parton, R. G. (2005). Ultrastructural identification of uncoated caveolin-independent early endocytic vehicles. *J. Cell Biol.* **168**, 465-476.

Kremer, J. R., Mastronarde, D. N. and McIntosh, J. R. (1996). Computer visualization of three-dimensional image data using IMOD. *J. Struct. Biol.* **116**, 71-76.

Lamaze, C., Dujeancourt, A., Baba, T., Lo, C. G., Benmerah, A. and Dautry-Varsat, A. (2001). Interleukin 2 receptors and detergent-resistant membrane domains define a clathrin-independent endocytic pathway. *Mol. Cell* **7**, 661-671.

Lemmon, S. K. and Traub, L. M. (2012). Getting in touch with the clathrin terminal domain. *Traffic* **13**, 511-519.

Liu, F. T., Bohn, J. W., Ferry, E. L., Yamamoto, H., Molinaro, C. A., Sherman, L. A., Klinman, N. R. and Katz, D. H. (1980). Monoclonal dinitrophenyl-specific murine IgE antibody: preparation, isolation, and characterization. *J. Immunol.* **124**, 2728-2737.

Liu, A. P., Aguet, F., Danuser, G. and Schmid, S. L. (2010). Local clustering of transferrin receptors promotes clathrin-coated pit initiation. *J. Cell Biol.* **191**, 1381-1393.

Mao, S. Y., Varin-Blank, N., Edidin, M. and Metzger, H. (1991). Immobilization and internalization of mutated IgE receptors in transfected cells. *J. Immunol.* **146**, 958-966.

Mao, S. Y., Pfeiffer, J. R., Oliver, J. M. and Metzger, H. (1993). Effects of subunit mutation on the localization to coated pits and internalization of cross-linked IgE-receptor complexes. *J. Immunol.* **151**, 2760-2774.

Martínez-Martín, N., Fernández-Arenas, E., Cemerski, S., Delgado, P., Turner, M., Heuser, J., Irvine, D. J., Huang, B., Bustelo, X. R., Shaw, A. et al. (2011). T cell receptor internalization from the immunological synapse is mediated by TC21 and RhoG GTPase-dependent phagocytosis. *Immunity* **35**, 208-222.

Mastronarde, D. N. (2005). Automated electron microscope tomography using robust prediction of specimen movements. *J. Struct. Biol.* **152**, 36-51.

McMahon, H. T. and Boucrot, E. (2011). Molecular mechanism and physiological functions of clathrin-mediated endocytosis. *Nat. Rev. Mol. Cell Biol.* **12**, 517-533.

Mellman, I. and Plutner, H. (1984). Internalization and degradation of macrophage Fc receptors bound to polyvalent immune complexes. *J. Cell Biol.* **98**, 1170-1177.

Molfetta, R., Gasparrini, F., Peruzzi, G., Vian, L., Piccoli, M., Frati, L., Santoni, A. and Paolini, R. (2009). Lipid raft-dependent FcepsilonRI ubiquitination regulates receptor endocytosis through the action of ubiquitin binding adaptors. *PLoS ONE* **4**, e5604.

Naslavsky, N., Weigert, R. and Donaldson, J. G. (2004). Characterization of a nonclathrin endocytic pathway: membrane cargo and lipid requirements. *Mol. Biol. Cell* **15**, 3542-3552.

Nossal, R. and Zimmerberg, J. (2002). Endocytosis: curvature to the ENTH degree. *Curr. Biol.* **12**, R770-R772.

Oliver, C., Fujimura, A., Silveira e Souza, A. M., Orlandini de Castro, R., Siraganian, R. P. and Jamur, M. C. (2007). Mast cell-specific gangliosides and FcepsilonRI follow the same endocytic pathway from lipid rafts in RBL-2H3 cells. *J. Histochem. Cytochem.* **55**, 315-325.

Paolini, R. and Kinet, J. P. (1993). Cell surface control of the multiubiquitination and deubiquitination of high-affinity immunoglobulin E receptors. *EMBO J.* **12**, 779-786.

Parachoniak, C. A. and Park, M. (2009). Distinct recruitment of Eps15 via Its coiled-coil domain is required for efficient down-regulation of the met receptor tyrosine kinase. *J. Biol. Chem.* **284**, 8382-8394.

Pasqualato, S., Ménétrey, J., Franco, M. and Cherfils, J. (2001). The structural GDP/GTP cycle of human Arf6. *EMBO Rep.* **2**, 234-238.

Peters, P. J., Hsu, V. W., Ooi, C. E., Finazzi, D., Teal, S. B., Oorschot, V., Donaldson, J. G. and Klausner, R. D. (1995). Overexpression of wild-type and mutant ARF1 and ARF6: distinct perturbations of nonoverlapping membrane compartments. *J. Cell Biol.* **128**, 1003-1017.

Pettersen, E. F., Goddard, T. D., Huang, C. C., Couch, G. S., Greenblatt, D. M., Meng, E. C. and Ferrin, T. E. (2004). UCSF Chimera – a visualization system for exploratory research and analysis. *J. Comput. Chem.* **25**, 1605-1612.

Polo, S. (2012). Signaling-mediated control of ubiquitin ligases in endocytosis. *BMC Biol.* **10**, 25.

Radhakrishna, H. and Donaldson, J. G. (1997). ADP-ribosylation factor 6 regulates a novel plasma membrane recycling pathway. *J. Cell Biol.* **139**, 49-61.

Ramanan, V., Agrawal, N. J., Liu, J., Engles, S., Toy, R. and Radhakrishnan, R. (2011). Systems biology and physical biology of clathrin-mediated endocytosis. *Integr. Biol. (Camb)* **3**, 803-815.

Sanan, D. A. and Anderson, R. G. (1991). Simultaneous visualization of LDL receptor distribution and clathrin lattices on membranes torn from the upper surface of cultured cells. *J. Histochem. Cytochem.* **39**, 1017-1024.

Sauvonnet, N., Dujeancourt, A. and Dautry-Varsat, A. (2005). Cortactin and dynamin are required for the clathrin-independent endocytosis of gammac cytokine receptor. *J. Cell Biol.* **168**, 155-163.
Schmid, S. L. and Frolov, V. A. (2011). Dynamin: functional design of a membrane fission catalyst. *Annu. Rev. Cell Dev. Biol.* **27**, 79-105.
Sigismund, S., Woelk, T., Puri, C., Maspero, E., Tacchetti, C., Transidico, P., Di Fiore, P. P. and Polo, S. (2005). Clathrin-independent endocytosis of ubiquitinated cargos. *Proc. Natl. Acad. Sci. USA* **102**, 2760-2765.
Sorkin, A. and von Zastrow, M. (2009). Endocytosis and signalling: intertwining molecular networks. *Nat. Rev. Mol. Cell Biol.* **10**, 609-622.
Stoddart, A., Jackson, A. P. and Brodsky, F. M. (2005). Plasticity of B cell receptor internalization upon conditional depletion of clathrin. *Mol. Biol. Cell* **16**, 2339-2348.
Sundborger, A., Soderblom, C., Vorontsova, O., Evergren, E., Hinshaw, J. E. and Shupliakov, O. (2011). An endophilin-dynamin complex promotes budding of clathrin-coated vesicles during synaptic vesicle recycling. *J. Cell Sci.* **124**, 133-143.
Torgersen, M. L., Skretting, G., van Deurs, B. and Sandvig, K. (2001). Internalization of cholera toxin by different endocytic mechanisms. *J. Cell Sci.* **114**, 3737-3747.
Traub, L. M. (2009). Tickets to ride: selecting cargo for clathrin-regulated internalization. *Nat. Rev. Mol. Cell Biol.* **10**, 583-596.
van Bergen en Henegouwen, P. M. (2009). Eps15: a multifunctional adaptor protein regulating intracellular trafficking. *Cell Commun. Signal.* **7**, 24.
van der Heide, P., Xu, X. P., Marsh, B. J., Hanein, D. and Volkmann, N. (2007). Efficient automatic noise reduction of electron tomographic reconstructions based on iterative median filtering. *J. Struct. Biol.* **158**, 196-204.
Volkmann, N. (2002). A novel three-dimensional variant of the watershed transform for segmentation of electron density maps. *J. Struct. Biol.* **138**, 123-129.
Volkmann, N. (2004). An approach to automated particle picking from electron micrographs based on reduced representation templates. *J. Struct. Biol.* **145**, 152-156.
Volkmann, N. and Hanein, D. (1999). Quantitative fitting of atomic models into observed densities derived by electron microscopy. *J. Struct. Biol.* **125**, 176-184.
von Kleist, L., Stahlschmidt, W., Bulut, H., Gromova, K., Puchkov, D., Robertson, M. J., MacGregor, K. A., Tomilin, N., Pechstein, A., Chau, N. et al. (2011). Role of the clathrin terminal domain in regulating coated pit dynamics revealed by small molecule inhibition. *Cell* **146**, 471-484.
Whitaker, R. T. and Xue, X. (2001). Variable-conductance, level-set curvature for image denoising. *Proc. Int. Conf. Image Proc.* **3**, 142-145.
Wilson, B. S., Pfeiffer, J. R. and Oliver, J. M. (2000). Observing FcepsilonRI signaling from the inside of the mast cell membrane. *J. Cell Biol.* **149**, 1131-1142.
Wilson, B. S., Pfeiffer, J. R., Surviladze, Z., Gaudet, E. A. and Oliver, J. M. (2001). High resolution mapping of mast cell membranes reveals primary and secondary domains of Fc(epsilon)RI and LAT. *J. Cell Biol.* **154**, 645-658.
Wilson, B. S., Pfeiffer, J. R. and Oliver, J. M. (2002). FcepsilonRI signaling observed from the inside of the mast cell membrane. *Mol. Immunol.* **38**, 1259-1268.
Wilson, B. S., Steinberg, S. L., Liederman, K., Pfeiffer, J. R., Surviladze, Z., Zhang, J., Samelson, L. E., Yang, L. H., Kotula, P. G. and Oliver, J. M. (2004). Markers for detergent-resistant lipid rafts occupy distinct and dynamic domains in native membranes. *Mol. Biol. Cell* **15**, 2580-2592.
Wilson, B. S., Pfeiffer, J. R., Raymond-Stintz, M. A., Lidke, D., Andrews, N., Zhang, J., Yin, W., Steinberg, S. and Oliver, J. M. (2007). Exploring membrane domains using native membrane sheets and transmission electron microscopy. *Methods Mol. Biol.* **398**, 245-261.
Xue, M., Hsieh, G., Raymond-Stintz, M. A., Pfeiffer, J., Roberts, D., Steinberg, S. L., Oliver, J. M., Prossnitz, E. R., Lidke, D. S. and Wilson, B. S. (2007). Activated N-formyl peptide receptor and high-affinity IgE receptor occupy common domains for signaling and internalization. *Mol. Biol. Cell* **18**, 1410-1420.
Zhang, J., Leiderman, K., Pfeiffer, J. R., Wilson, B. S., Oliver, J. M. and Steinberg, S. L. (2006). Characterizing the topography of membrane receptors and signaling molecules from spatial patterns obtained using nanometer-scale electron-dense probes and electron microscopy. *Micron* **37**, 14-34.
Zwang, Y. and Yarden, Y. (2009). Systems biology of growth factor-induced receptor endocytosis. *Traffic* **10**, 349-363.

Journal of Cell Science

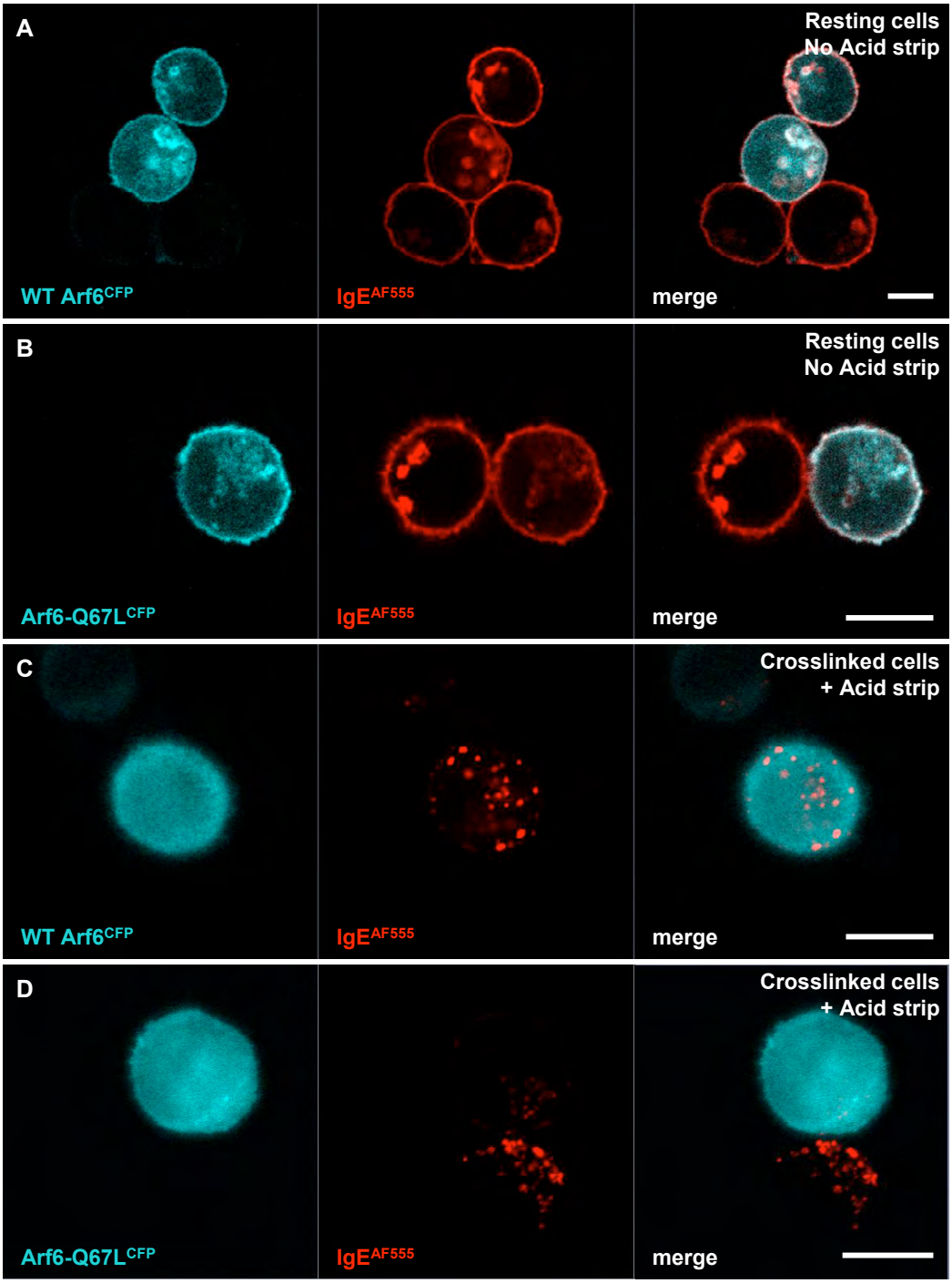

Fig. S1. Expression of mutant Arf6 alter Fc ε RI internalization but not IgE binding. RBL cells transiently transfected with WT Arf6^{CFP} (**A,C**) or Arf6-Q67L^{CFP} (**B,D**) were primed with IgE^{AF555} and crosslinked (**C-D**), or not (**A-B**), with DNP^{24} for 10' at 37°C before fixation and imaging. Scale bars = 10 μ m.

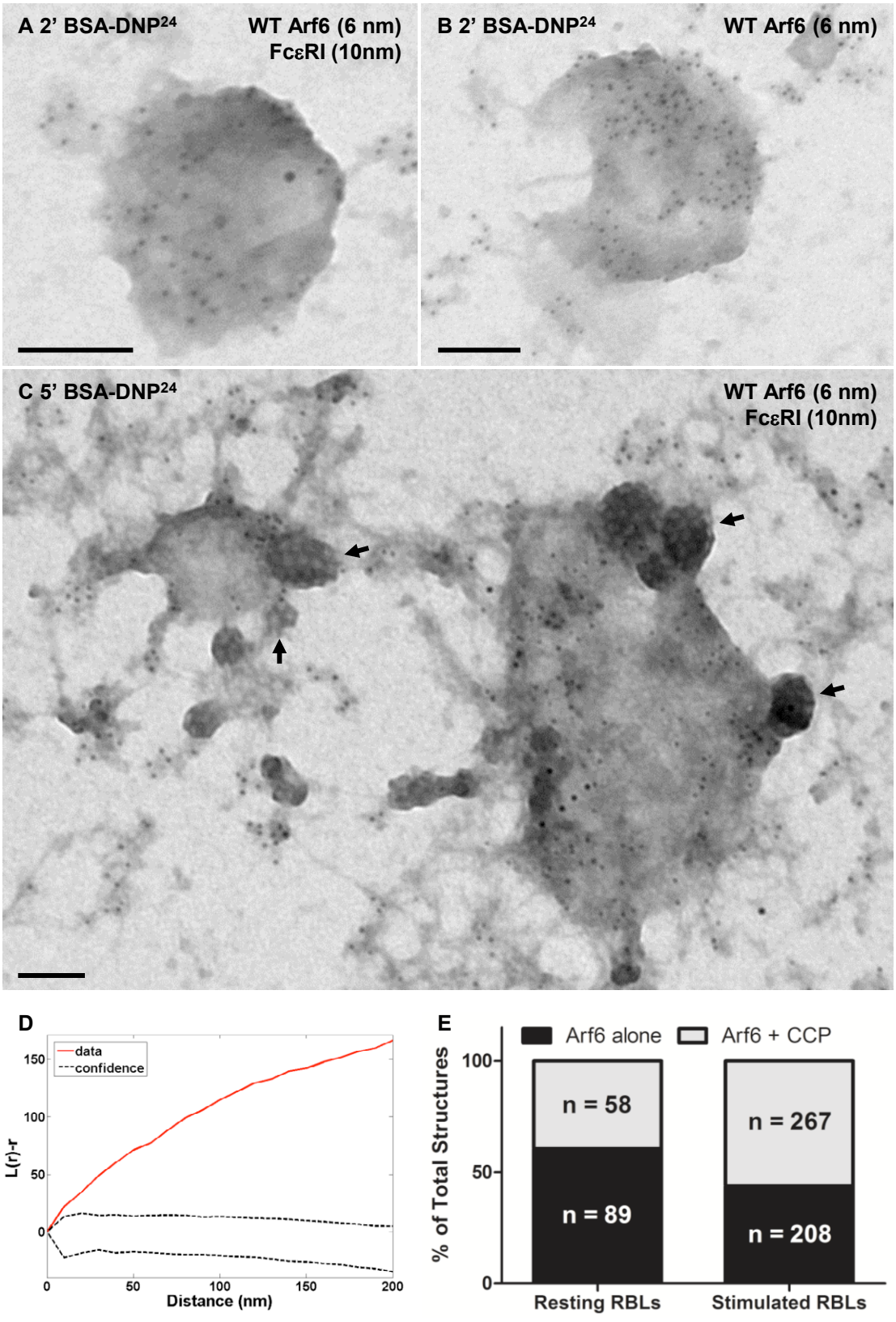

Fig. S2. Arf6 positive structures are often with/connected to CCP. (**A-C**) TEM image of membrane sheets prepared from cells expressing WT Arf6^{CFP} (6 nm gold). Samples were primed with IgE and stimulated for 2' (**A-B**) or 5' (**C**) with DNP-gold (10 nm gold). (**D**) Ripley's bivariate statistical co-clustering test corresponding to images (**C**). (**E**) Quantification of Arf6 structures alone or connected to a CCP in resting or stimulated RBLs. Scale bars = 100 nm (A-C).

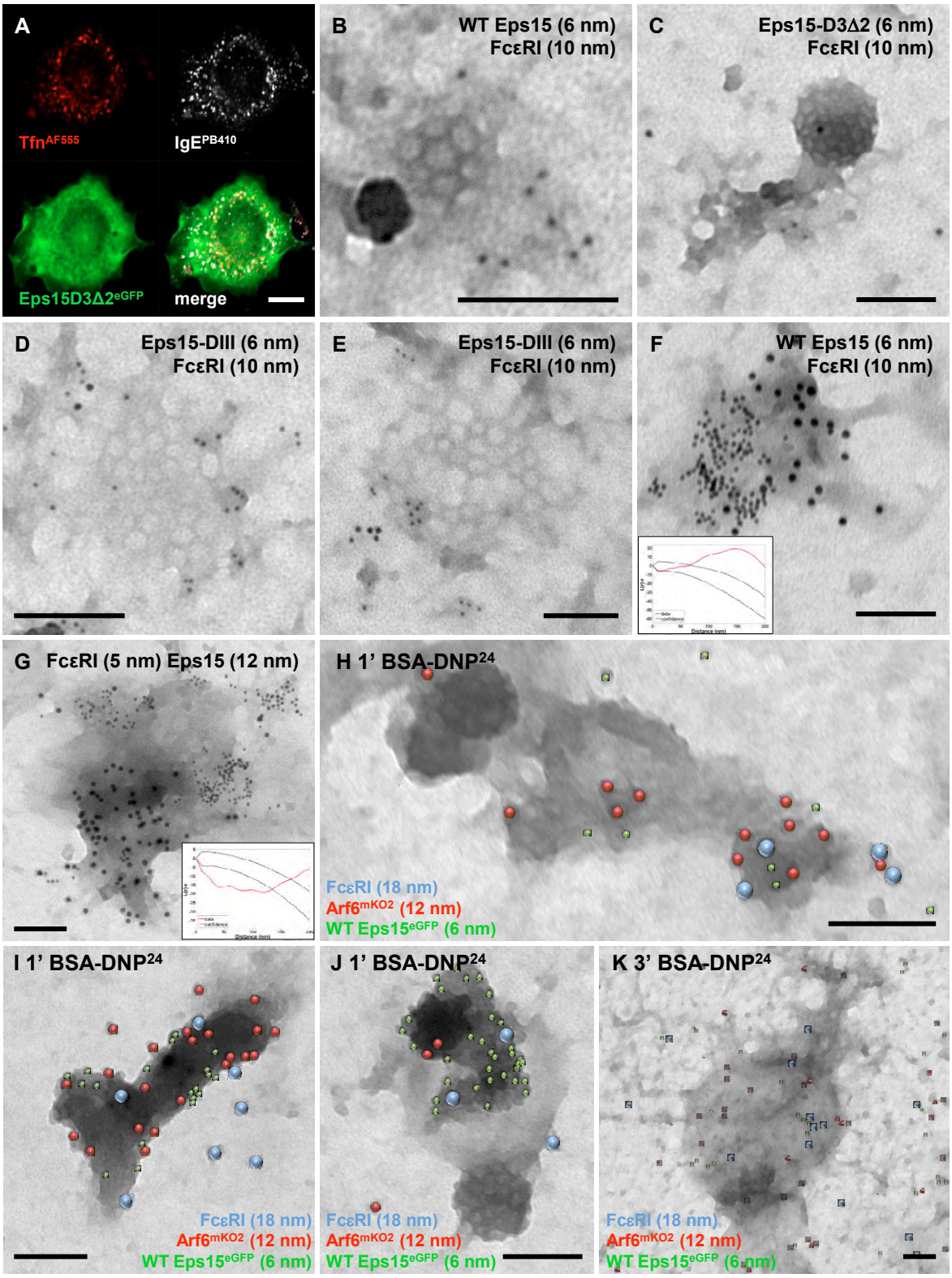

Fig. S3. Expression of a dominant negative Eps15 increase the occurrence of flat clathrin coated pits. (**A**) Confocal image of RBL cells transiently transfected with Eps15 D3 Δ 2^{eGFP} primed with IgE^{PB410} and stimulated with DNP^{24} and tfn^{AF555} (Invitrogen) for 10' at 37°C. (**B-G**) Electron micrograph of RBL-2H3 cells expressing WT Eps15^{eGFP} (**B**,**F-G**), Eps15 D3 Δ 2^{eGFP} (**C**) or Eps15 DIII^{eGFP} (**D-E**) (6 nm gold); primed with IgE and stimulated with DNP-gold before imaging. Insert graph on images **F** and **G** are Ripley's bivariate statistical co-clustering test for Eps15 and Fc ε RI. (**H-K**) Electron micrographs of membrane sheets triply labelled for WT Eps15^{eGFP} (6 nm gold, green dots), Arf6^{mKO2} (12 nm gold, red dots) and Fc ε RIβ (18 nm gold, blue dots) after 1' (**H-J**) or 3' (**K**) stimulation at 37°C. Scale bars = 10 μ m (**A**) or 100 nm (**B-K**).

Movie 1. Z-slices throughout a RBL cells (showed in Fig. **1G**) primed with IgE^{AF488} and stimulated with DNP^{24} and tfn^{AF555} (Invitrogen) for 10' at 37°C, showing the complete internalization of both transferrin and IgE receptors. Scale bar = 5 μ m.

Movie 2. Z-slices throughout a RBL cells (showed in Fig. **1H**) primed with IgE^{AF488} and stimulated with DNP^{24} and tfn^{AF555} (Invitrogen) for 10' at 37°C, beforehand treated with siRNA anti-clathrin HC, showing the complete internalization of the IgE receptors while transferrin stays on the cell surface. Scale bar = 5 μ m.

Movie 3 and 4. 3D EM reconstructions of the Arf6 structures observed in Figure **3D** and **G**.

Movie 5. 3D EM reconstruction of a clathrin coated pit with WT Dynamin gold labels present at the neck of the vesicle.

Movie 6. Z-stack maximum intensity projection of a RBL cell stably expressing WT Dynamin^{eGFP} and primed with IgE^{AF555} showing a diffuse and homogeneous distribution of WT Dynamin^{eGFP}. Scale bar = 5 μ m.

Movie 7. Z-stack maximum intensity projection of a RBL cell stably expressing Dynamin-K44A^{eGFP} and primed with IgE^{AF555}, showing the presence of Dynamin-K44A^{eGFP} in punctate structures near the cell surface. Scale bar = 5 μ m.

Movie 8. Z-stack maximum intensity projection of a RBL cell transiently expressing WT Eps15^{eGFP} showing the accumulation of bright Eps15 structures connected, or next, to the plasma membrane. Scale bar = 10 μ m.

Movie 9 and 10. 3D EM reconstructions of the Eps15 structures observed in Figure **7A** and **D**.

Movie 11. Z-stack maximum intensity projection of the RBL cell presented in Figure **8G,** showing a high degree of Fc ε RI internalization after crosslinking with DNP^{24}-BSA Scale bar = 5 μ m.

Movie 12 Z-stack maximum intensity projection of the RBL cell presented in Figure **8I**, showing the accumulation of aggregated Fc ε RI on the cell surface and the absence of internalization upon crosslinking with DNP^{24}-BSA after a 30' treatment with Pitstop2 at 60 μ M. Scale bar = 5 μ m.